Main Manuscript for

Title

Paradoxical Tumor Suppressor Role of Yorkie Through a TOR-Dependent α-Tubulin Acetylation in Select Squamous Epithelium

Running title

Lineage-specific tumor suppressor role of Yki

Authors

Rachita Bhattacharya[1, 4], Jeganath Ammavasai[1], Shruti Agarwal[1, 2], Hamim Zafar[1, 2, 3], Pradip Sinha[1, *], and Nitin Mohan[1, *]

[1]Biological Sciences and Bioengineering, [2]Mehta Family Center for Engineering in Medicine, [3]Computer Science and Engineering, Indian Institute of Technology Kanpur, India
[4]Current address: Genetics and Developmental Biology Unit, Institut Curie, CNRS UMR 3215, INSERM U934, Paris, France

*Corresponding authors: Pradip Sinha and Nitin Mohan
Email: pradips@iitk.ac.in, nitinm@iitk.ac.in

Author Contributions: Conceptualization: RB, NM, PS. Data acquisition: RB, JA. Transcriptomic analysis: RB, SA, HZ. Manuscript draft, edits, and revision: RB, NM, PS.
Competing Interest Statement: The authors declare no conflict of interest.
Classification: Biological Sciences, Developmental Biology
Keywords: Yorkie, TOR, microtubule acetylation, squamous cell carcinoma.
This file includes:
Main Text with References
Figure Legends

Abstract

Protooncogenes, which can also function as tumor suppressors, are termed double agents. The Hippo pathway transcriptional coactivators YAP/TAZ and their *Drosophila* homolog Yorkie (Yki) are known oncogenes. Paradoxically, in squamous epithelia, they are constitutively active yet non-oncogenic and can even function as tumor suppressors. We previously found that loss of Yki in the *Drosophila* male accessory gland (MAG) squamous epithelium promotes squamous cell carcinoma (SCC) by upregulating TOR signaling, but the mechanism was unknown. Here, we show that this tumorigenesis stems from TOR-mediated hyperacetylation of α-tubulin. This pathway is tissue-specific, as the ovarian follicular epithelium is resistant to Yki loss. A comparison of MAG and follicular epithelia single-cell transcriptomic data revealed their distinct Yki-TOR signaling states, suggesting lineage-specific mechanoconstraints in these two lineages. Our results identify suppression of TOR-driven α-tubulin acetylation as the mechanistic basis for Yki's role as a double-agent in select squamous epithelia.

Introduction

Some protooncogenes can function as tumor suppressors in specific cell types. Examples include NOTCH1 (Lobry et al., 2014), TP53/p53 (Soussi and Wiman, 2015), or RB1(Chau and Wang, 2003). Such genes are described as “double agents” due to their context-specific opposing roles in carcinogenesis (Shen et al., 2018). YAP/TAZ in mammals, and Yorkie (Yki) in *Drosophila*, are also protooncogenes. Out-of-context activation of these proteins promotes cancer (Huang et al., 2005; Zanconato et al., 2016). However, in squamous epithelia, nuclear YAP/TAZ/Yki signaling is perpetual. This is due to cell flattening, which provides a mechanosensory relief from their cytoplasmic sequestration (Dupont et al., 2011; Fletcher et al., 2018; Kowalczyk et al., 2022; Nakajima et al., 2017). Such a scenario of developmentally programmed and chronic YAP/TAZ/Yki signaling likely occludes its protooncogenic roles in select squamous epithelia. For instance, loss of YAP/TAZ signaling results in lung squamous cell carcinoma (Gao et al., 2014; Huang et al., 2017), thereby revealing its tumor-suppressor-like role (Pearson et al., 2021)(for review, see (Baroja et al., 2024; Franklin et al., 2023; Luo et al., 2023)). Recently, we have shown that in *Drosophila*, too, loss of Yki signaling in the squamous epithelium of the male accessory gland (MAG) triggers TOR signaling and induces re-entry into the cell cycle, culminating in squamous cell carcinoma (SCC) (Bhattacharya et al., 2024). This outcome contrasts with the follicular squamous epithelium (Borreguero-Muñoz et al., 2019; Fletcher et al., 2018), where loss of Yki signaling fails to trigger SCC, even though nuclear Yki signaling is a common feature of both these epithelial types. Thus, Yki, like its human counterparts YAP/TAZ, displays the hallmarks of a double agent in select cell types. Yet the mechanistic

basis of its paradoxical tumor suppressor activity—specifically how Yki restrains TOR-driven processes to prevent carcinoma in squamous epithelia—remains unresolved.

Several lines of recent evidence suggest a hitherto unexplored possibility of a tumor suppressor-like role of developmentally programmed nuclear Yki signaling in select squamous epithelia. For example, Hippo signaling is regulated by microtubule acetylation (Mok and Choi, 2022), which is required for cell stretching or flattening (Moise et al., 2024; Seetharaman et al., 2022) and also implicated in carcinogenesis (Wattanathamsan and Pongrakhananon, 2023). We therefore asked whether a Yki–TOR–microtubule acetylation axis explains MAG-SCC. Here, we test this hypothesis and uncover a lineage-specific mechanism in which suppression of TOR-driven α-tubulin acetylation underlies Yki's paradoxical role as a double-agent tumor suppressor in *Drosophila* squamous epithelium.

Results

Microtubule acetylation is required for squamous cell flattening

Because epithelial stretching correlates with microtubule acetylation *in vitro*, we examined its endogenous levels during *Drosophila* follicular and MAG epithelial flattening. In both, the columnar-to-squamous transition coincided with elevated microtubule acetylation (**Fig. 1A–B and Fig. 1—figure supplement 1A-D**). In the ovarian follicular epithelium, for instance, total α-tubulin and acetylated microtubule levels rose in parallel during the columnar-to-squamous transition, suggesting near-complete acetylation of the tubulin pool in flattened squamous cells (**Fig. 1—figure supplement 2A–D**).

To test the functional significance of this acetylation, we knocked down *α-tat* (which encodes α-tubulin acetyltransferase). Loss of *α-tat* activity did not affect total α-tubulin organization or density (**Fig. 1—figure supplement 3A–B**), but reduced cell area in both follicular (*GR1-Gal4>α-tat-IR*, **Fig. 1C and Fig. 1—figure supplement 1E**) and MAG (*ov-Gal4>α-tat-IR*, **Fig. 1D and Fig. 1—figure supplement 1F**) squamous epithelia. Loss of cell flattening was accompanied by corresponding decreases in organ size in both the MAG and egg chambers (**Fig. 1D**, top panel; **Fig. 1—figure supplement 3C–D**). These results establish a foundation to explore how tubulin acetylation impacts additional cellular processes integral to squamous morphogenesis. Thus, we next investigated how microtubule acetylation affects membrane protein trafficking during epithelial flattening.

α-tat loss disrupts junctional protein localization and actin organization

Cell flattening during squamous cell morphogenesis reduces cell–cell adhesion (Gomez et al., 2012). We also noticed low levels of the lateral membrane protein FasIII (Wells et al., 2013),

95 the sub-apical adherens junction protein, DE-Cadherin (Huang et al., 2012; Pope and Harris,
96 2008), and the basolateral protein, Lgl (Bilder et al., 2000) (**Fig. 2—figure supplement 1A-**
97 **I**) during the cuboidal-to-squamous transition of follicular epithelium. Therefore, these
98 proteins likely redistribute or are substantially reduced from the cell junctions during the
99 cuboidal-to-squamous transition. Since *α-tat* knockdown impaired cell-flattening (**Fig. 1C-**
100 **D**), we next analyzed its effect on membrane protein trafficking during epithelial
101 morphogenesis. We knocked down *α-tat* in somatic clones (*hs-flp, act>α-tat-IR*). Compared
102 with controls (**Fig. 2A-D′, blue asterisk**), *α-tat* knockdown reduced cell size and increased
103 cadherin localization at cell boundaries in both follicular (**Fig. 2B, B′** (red asterisk) and **Fig.**
104 **2—figure supplement 2A**) and MAG epithelia (**Fig. 2D, D′** (red asterisk) and **Fig. 2—figure**
105 **supplement 2B**). Likewise, FasIII and Lgl accumulated at clone boundaries (*hs-flp, act>α-*
106 *tat-IR*) (**Fig. 2—figure supplement 3A–H**).
107 To further explore the consequences on vesicular trafficking, we analysed endosomal protein
108 localization in *α-tat* knockdown somatic clones (*hs-flp, act>α-tat-IR*) in Stage 14 follicular
109 epithelium. Sequestration of these membrane proteins was accompanied by peripheral
110 accumulation of early endosomes (Rab5) containing Lgl (**Fig. 2—figure supplement 4A–C**),
111 a phenotype resembling the defective Fasciclin 2 trafficking reported upon Tao kinase
112 knockdown during the columnar-to-squamous transition (Gomez et al., 2012). Microtubule
113 acetylation, therefore, appears critical for the endocytic trafficking of membrane proteins
114 during epithelial cell flattening.
115 To further probe the role of microtubule acetylation on the actin cytoskeleton, we knocked
116 down *α-tat* in MAG and ovarian follicular epithelium. In follicular epithelium, *α-tat*
117 knockdown increased levels of the actin-severing protein cofilin (*hs-flp, act>α-tat-IR*, **Fig.**
118 **2E**), which likely explains their depolymerization of actin (phalloidin, **Fig. 2F**). Similarly, *α-*
119 *tat* knockdown in the MAG epithelium led to sparse and depolymerized actin structures
120 (*ov>UAS-Life-Actin RFP*, *α-tat-IR*, **Fig. 2G**). Thus, loss of microtubule acetylation impairs
121 both membrane protein transport and actin polymerization, which are essential processes for
122 cell flattening in squamous epithelia (**Fig. 2H**). In essence, microtubule acetylation is critical
123 for cell flattening, likely by promoting endocytic trafficking and actin polymerization.

124 ***Tissue-specific crosstalk between Yki signaling and microtubule acetylation***
125 Microtubule hyperacetylation is a recognized prognostic marker in carcinomas, including
126 SCC (Wattanathamsan and Pongrakhananon, 2023). We therefore hypothesized that Yki-
127 mediated repression of TOR signaling restrains tumor-promoting microtubule acetylation.
128 However, we noted that while in both follicular and MAG squamous epithelia, Yki exhibits

129 nuclear localisation (Yki-GFP, **Fig. 3A–B**), the fallouts of its knockdowns were disparate. In
130 the MAG, *yki* knockdown increased cell area (**Fig. 3—figure supplement 1A–C**, readout of
131 enhanced TOR signaling (Bhattacharya et al., 2024)) with accompanying elevated
132 microtubule acetylation (**Fig. 3C–E**), cytoarchitectural disruption (**Fig. 3F**), while *α-tat*
133 knockdown reduced microtubule acetylation in *yki*-knockdown MAG (*ov>tat-IR, yki-IR;*
134 **Fig. 3E**), and suppressed MAG-SCC (**Fig. 3F-G**) and extended host lifespan (**Fig. 3H**). By
135 contrast, in the follicular epithelium, *yki* knockdown reduced cell size (**Fig. 3—figure**
136 **supplement 1D–E)** and downregulated acetylated microtubules (**Fig. 3I–J**).
137 As predicted by this model, gain of TOR signaling in the MAG (*ov>myr-Akt*, **Fig. 3K**) or
138 follicular epithelium (*c204>myr-Akt*, **Fig. 3L**) increased microtubule acetylation. Conversely,
139 TOR downregulation in the MAG (*ov>Akt-IR*, **Fig. 3M**) or follicle (*c204>Akt-IR*, **Fig. 3N**)
140 decreased acetylation, confirming TOR as a direct regulator of microtubule acetylation *in*
141 *vivo*.
142 The mechanism of TOR-dependent acetylation is likely conserved. We noted that
143 mammalian ATAT1, the homolog of *Drosophila* α-tat, contains conserved AKT3- and pS6K-
144 phosphorylation sites (**Fig. 3—figure supplement 2A**). Furthermore, in mammalian BS-C-1
145 cells, treatment with the TOR inhibitor rapamycin reduced microtubule acetylation (**Fig. 3—**
146 **figure supplement 2B-C**). These findings suggest a conserved pathway for TOR-mediated
147 regulation of α-tubulin acetylation.
148 Together, a Yki-dependent regulation of TOR signaling (and consequently microtubule
149 acetylation), as seen in the MAG, shows a causal underpinning of the cell type-specific tumor
150 suppressor role of Yki.

151 ***A developmental priming of the Yki-TOR-microtubule acetylation axis***
152 The absence of TOR-mediated microtubule hyperacetylation upon *yki* knockdown in
153 follicular epithelium suggests tissue-specific developmental priming. To test this possibility,
154 we analyzed single-cell transcriptomic data from 44,544 integrated cells of both tissues (Fly
155 Cell Atlas). Out of twelve annotated cell clusters (**Fig. 4A**, see *Supporting Information*), we
156 focused on MAG main cells and stage 14 choriogenic main-body follicle cells (**Fig. 4B**). Our
157 analysis revealed that, compared to MAG squamous epithelia, follicular epithelium showed
158 higher baseline expression of TOR-pathway genes (S6k, PDK1, Pten, Mitf, PI3K21B) and
159 Insulin-pathway genes (rl, InR, foxo, chico, Ilp8, ImpL2) (**Fig. 4C**), consistent with their
160 roles in supporting intense biosynthetic demands of chorion formation and oocyte growth
161 (Das and Arur, 2017). In MAG, a relatively lower TOR/Insulin signaling may reflect
162 evolutionary prioritization of nutrient allocation toward oogenesis over sex-peptide

163 production. Follicular cells also exhibited elevated expression of the TEAD transcription
164 factor Sd and its downstream effector Diap1 (**Fig. 4C**), indicating a Yki-linked pro-survival
165 bias. We propose that these transcriptional differences arise from the distinct
166 mechanostresses of each tissue (Gullekson et al., 2017; Hannezo and Heisenberg, 2019).

167 **Discussion**

168 Protooncogenes like YAP/TAZ/Yki can function as context-dependent tumor suppressors
169 (for review, see (Baroja et al., 2024; Franklin et al., 2023; Luo et al., 2023)), or "double
170 agents" (Shen et al., 2018) but the mechanisms behind this duality have remained elusive.
171 Here, we identify the suppression of TOR-driven α-tubulin acetylation as the mechanistic
172 basis for Yorkie's (Yki) tumor suppressor role in the *Drosophila* male accessory gland
173 (MAG) squamous epithelium.

174 Variations in substrate stiffness affect mechanochemical sensing (Hannezo and Heisenberg,
175 2019). Tissue-specific outcomes of Yki loss seen here likely mirror this mechanochemical
176 distinctiveness of MAG and follicular squamous epithelium. Previously, it was also shown
177 that higher substrate stiffness enhances α-tubulin acetylation, actin bundling, and YAP/TAZ
178 nuclear entry (Seetharaman et al., 2022). While both MAG and follicular epithelia exhibit
179 constitutive nuclear Yki, only the MAG develops carcinoma upon Yki loss, suggesting that
180 their disparate substrate stiffness may underlie this differential tumor susceptibility. This
181 interpretation is corroborated by the distinctiveness between the two tissues. First, the MAG
182 epithelium faces a fluid-filled lumen, whereas the follicular epithelium interfaces with a rigid
183 chorion enveloping the oocyte. Second, our single-cell transcriptomics revealed that follicular
184 cells are developmentally primed with high baseline TOR/Insulin signaling and Yki-target
185 gene expression, likely fulfilling the biosynthetic demands of oogenesis. In contrast, MAG
186 epithelium relies on Yki to actively restrain the TOR-α-tubulin acetylation axis, making it
187 uniquely susceptible to Yki-loss-induced SCC (**Fig. 4D**).

188 Our findings integrate several isolated pillars of human SCC pathogenesis. For instance, in
189 alveolar type 1 (AT1) lung cells, nuclear YAP/TAZ activity restrains TOR signaling and
190 maintains cell homeostasis (Ohnishi et al., 2024), oncogenic PI3K-Akt-TOR signaling is a
191 known driver of SCCs (Zheng et al., 2024), and α-tubulin acetylation promotes SCC
192 aggressiveness and chemoresistance (Wattanathamsan and Pongrakhananon, 2023). Our
193 findings provide a unified, causal pathway linking these elements: the loss of a Yki signaling
194 "double agent" triggers TOR signaling, which in turn drives microtubule hyperacetylation to
195 cause carcinoma. By delineating the Yki-TOR-α-tubulin acetylation axis, we provide a

196 mechanistic model for how "double-agent" protooncogenes can suppress cancer in specific
197 tissues, revealing new potential avenues for therapeutic intervention in squamous cell
198 carcinomas.

199 **MATERIALS AND METHODS**

200 All the genetic stocks and reagents used in this study have been procured from public
201 repositories or as gifts from other researchers. Details of the experiments, for instance,
202 *Drosophila* maintenance and induction of transgenes, immunostaining protocol, mammalian
203 cell culture-based protocol, microscopy, quantification, statistical analysis, bioinformatics,
204 and scRNA sequence analysis, are provided in the *Supporting Information Appendix.*

205 **DATA AVAILABILITY**

206 All data generated during this study are included in this article. Additionally, publicly
207 available data from the Fly Cell Atlas were analyzed in this research.

208 **FUNDING**

209 Science and Engineering Research Board, SERB/CRG/2022/00839: NM, PS
210 Science and Engineering Research Board, SERB/CRG/2019/00324: NM
211 Department of Science and Technology, EMR/2016/006723: PS
212 Department of Biotechnology, BT/13/IYBA/2020/05: HZ
213 Indian Council of Medical Research, 3/1/3/JRF-2015/HRD-138(30373): RB

214 **ACKNOWLEDGEMENTS**

215 We thank Barry Thompson, Kristipati Ravi Ram, and Mohit Prasad for fly stocks, and Jonaki
216 Sen for the cofilin antibody. We also thank Debdeep Dutta, Thamarailingam Athilingam, and
217 Saurabh Singh Parihar for their critical manuscript reading.

218

219 **REFERENCES**

220 **Baroja, I., Kyriakidis, N. C., Halder, G. and Moya, I. M.** (2024). Expected and
221 unexpected effects after systemic inhibition of Hippo transcriptional output in cancer.
222 *Nat. Commun.* **15**, 2700.
223 **Bhattacharya, R., Kumari, J., Banerjee, S., Tripathi, J., Parihar, S. S., Mohan, N. and**
224 **Sinha, P.** (2024). Hippo effector, Yorkie, is a tumor suppressor in select Drosophila
225 squamous epithelia. *Proc. Natl. Acad. Sci. U.S.A.* **121**, e2319666121.
226 **Bilder, D., Li, M. and Perrimon, N.** (2000). Cooperative regulation of cell polarity and

227 growth by Drosophila tumor suppressors. *Science* **289**, 113–116.
228 **Borreguero-Muñoz, N., Fletcher, G. C., Aguilar-Aragon, M., Elbediwy, A., Vincent-**
229 **Mistiaen, Z. I. and Thompson, B. J.** (2019). The Hippo pathway integrates PI3K–Akt
230 signals with mechanical and polarity cues to control tissue growth. *PLoS Biol* **17**,
231 e3000509.
232 **Chau, B. N. and Wang, J. Y. J.** (2003). Coordinated regulation of life and death by RB. *Nat.*
233 *Rev. Cancer* **3**, 130–138.
234 **Das, D. and Arur, S.** (2017). Conserved insulin signaling in the regulation of oocyte growth,
235 development, and maturation. *Mol. Reprod. Dev.* **84**, 444–459.
236 **Dupont, S., Morsut, L., Aragona, M., Enzo, E., Giulitti, S., Cordenonsi, M., Zanconato,**
237 **F., Le Digabel, J., Forcato, M., Bicciato, S., et al.** (2011). Role of YAP/TAZ in
238 mechanotransduction. *Nature* **474**, 179–184.
239 **Fletcher, G. C., Diaz-de-la-Loza, M.-D.-C., Borreguero-Muñoz, N., Holder, M., Aguilar-**
240 **Aragon, M. and Thompson, B. J.** (2018). Mechanical strain regulates the Hippo
241 pathway in Drosophila. *Development* **145**, dev159467.
242 **Franklin, J. M., Wu, Z. and Guan, K. L.** (2023). Insights into recent findings and clinical
243 application of YAP and TAZ in cancer. *Nat. Rev. Cancer* **23**, 512–525.
244 **Gao, Y., Zhang, W., Han, X., Li, F., Wang, X., Wang, R., Fang, Z., Tong, X., Yao, S., Li,**
245 **F., et al.** (2014). YAP inhibits squamous transdifferentiation of Lkb1-deficient lung
246 adenocarcinoma through ZEB2-dependent DNp63 repression. *Nat. Commun.* **5**, 4621.
247 **Gomez, J. M., Wang, Y. and Riechmann, V.** (2012). Tao controls epithelial morphogenesis
248 by promoting Fasciclin 2 endocytosis. *J. Cell Biol.* **199**, 1131–43.
249 **Gullekson, C., Walker, M., Harden, J. L. and Pelling, A. E.** (2017). Measuring
250 mechanodynamics in an unsupported epithelial monolayer grown at an air-water
251 interface. *Mol. Biol. Cell* **28**, 111–119.
252 **Hannezo, E. and Heisenberg, C. P.** (2019). Mechanochemical feedback loops in
253 development and disease. *Cell* **178**, 12–25.
254 **Huang, J., Wu, S., Barrera, J., Matthews, K. and Pan, D.** (2005). The Hippo Signaling
255 Pathway Coordinately Regulates Cell Proliferation and Apoptosis by Inactivating
256 Yorkie, the Drosophila Homolog of YAP. *Cell* **122**, 421–434.
257 **Huang, J., Huang, L., Chen, Y. J., Austin, E., Devor, C. E., Roegiers, F. and Hong, Y.**
258 (2012). Differential regulation of adherens junction dynamics during apical-basal
259 polarization. *Development* **139**, 4001–4013.
260 **Huang, H., Zhang, W., Pan, Y., Gao, Y., Deng, L., Li, F., Li, F., Ma, X., Hou, S., Xu, J.,**
261 **et al.** (2017). YAP suppresses lung squamous cell carcinoma progression via

262 deregulation of the DNP63-GPX2 axis and ROS accumulation. *Cancer Res.* **77**, 5769–
263 5781.
264 **Kowalczyk, W., Romanelli, L., Atkins, M., Hillen, H., González-Blas, C. B., Jacobs, J.,**
265 **Xie, J., Soheily, S., Verboven, E., Moya, I. M., et al.** (2022). Hippo signaling instructs
266 ectopic but not normal organ growth. *Science* **378**, eabg3679.
267 **Lobry, C., Oh, P., Mansour, M. R., Thomas Look, A. and Aifantis, I.** (2014). Notch
268 signaling: Switching an oncogene to a tumor suppressor. *Blood* **123**, 2451–2459.
269 **Luo, J., Deng, L., Zou, H., Guo, Y., Tong, T., Huang, M., Ling, G. and Li, P.** (2023).
270 New insights into the ambivalent role of YAP/TAZ in human cancers. *J. Exp. Clin.*
271 *Cancer Res.* **42**, 1–22.
272 **Moise, K., Arun, K. M., Pillai, M., Salvador, J., Mehta, A. S., Goyal, Y. and Iruela-**
273 **Arispe, M. L.** (2024). Endothelial cell elongation and alignment in response to shear
274 stress requires acetylation of microtubules. *Front. Physiol.* **15**, 1–17.
275 **Mok, J. W. and Choi, K. W.** (2022). Modulation of Hippo signaling by Mnat9 N-
276 acetyltransferase for normal growth and tumorigenesis in Drosophila. *Cell Death Dis.*
277 **13**, 1–7.
278 **Nakajima, H., Yamamoto, K., Agarwala, S., Terai, K., Fukui, H., Fukuhara, S., Ando,**
279 **K., Miyazaki, T., Yokota, Y., Schmelzer, E., et al.** (2017). Flow-Dependent
280 Endothelial YAP Regulation Contributes to Vessel Maintenance. *Dev. Cell* **40**, 523–536.
281 **Ohnishi, Y., Masui, A., Suezawa, T., Mikawa, R., Hirai, T., Hagiwara, M. and Gotoh, S.**
282 (2024). Screening of factors inducing alveolar type 1 epithelial cells using human
283 pluripotent stem cells. *Stem Cell Reports* **19**, 529–544.
284 **Pearson, J. D., Huang, K., Pacal, M., McCurdy, S. R., Lu, S., Aubry, A., Yu, T.,**
285 **Wadosky, K. M., Zhang, L., Wang, T., et al.** (2021). Binary pan-cancer classes with
286 distinct vulnerabilities defined by pro- or anti-cancer YAP/TEAD activity. *Cancer Cell*
287 **39**, 1115–1134.
288 **Pope, K. L. and Harris, T. J. C.** (2008). Control of cell flattening and junctional
289 remodelling during squamous epithelial morphogenesis in Drosophila. *Development*
290 **135**, 2227–2238.
291 **Seetharaman, S., Vianay, B., Roca, V., Farrugia, A. J., De Pascalis, C., Boëda, B.,**
292 **Dingli, F., Loew, D., Vassilopoulos, S., Bershadsky, A., et al.** (2022). Microtubules
293 tune mechanosensitive cell responses. *Nat. Mater.* **21**, 366–377.
294 **Shen, L., Shi, Q. and Wang, W.** (2018). Double agents: Genes with both oncogenic and
295 tumor-suppressor functions. *Oncogenesis* **7**, 25.
296 **Soussi, T. and Wiman, K. G.** (2015). TP53: An oncogene in disguise. *Cell Death Differ.* **22**,

1239–1249.

Wattanathamsan, O. and Pongrakhananon, V. (2023). Post-translational modifications of tubulin: their role in cancers and the regulation of signaling molecules. *Cancer Gene Ther.* **30**, 521–528.

Wells, R. E., Barry, J. D., Warrington, S. J., Cuhlmann, S., Evans, P., Huber, W., Strutt, D. and Zeidler, M. P. (2013). Control of tissue morphology by Fasciclin III-mediated intercellular adhesion. *Dev.* **140**, 3858–3868.

Zanconato, F., Cordenonsi, M. and Piccolo, S. (2016). YAP/TAZ at the roots of cancer. *Cancer Cell* **29**, 783–803.

Zheng, S., He, S., Liang, Y., Tan, Y., Liu, Q., Liu, T. and Lu, X. (2024). Understanding PI3K/Akt/mTOR signaling in squamous cell carcinoma: mutated PIK3CA as an example. *Mol. Biomed.* **5**, 13.

Figure Legends:

Figure 1. **Microtubule acetylation is elevated in squamous epithelia and required for cell flattening.**

(**A**) Follicle epithelium development (Top). Ovariole showing the transition from columnar (Stage 10) to squamous (Stage 14) morphology, visualized with a Cadherin reporter (*shg-mTomato*). (Bottom) Immunostaining reveals increased acetylated α-tubulin levels in Stage 14 squamous cells compared to Stage 10 columnar cells.

(**B**) Pupal (90h APF)-to-adult (7D) development of the male accessory gland (MAG) squamous epithelium, showing increased acetylated α-tubulin levels during columnar-to-squamous transition.

(**C**, **D**) Knockdown of *α-tat* impairs cell flattening in both Stage 14 follicle cells (C, *GR1-Gal4>α-tat-IR*) and adult MAG epithelium (D*, ov-Gal4>α-tat-IR*). Insets magnified below.

Abbreviation in this and all subsequent figures: G=germarium, S=Stage of oocytes, C=Columnar epithelium, MAG= male accessory gland, Acet-MT=acetylated microtubules, IR=RNAi, h=hours, APF=after pupa formation, D=days.

Scale bars: upper panels (A–B) 100 µm; lower panels (A, B) and all insets 10 µm.

Figure 2. *α-tat* knockdown alters junctional assembly and actin organization in squamous epithelia.

(**A**, **B**) Stage 14 ovarian follicular squamous epithelium displaying control (A, A') and *α-tat* knockdown (B, B') clones (marked by nuclear GFP). DE-Cad (*shg-mtomato* reporter) marks

331 cell outlines. Compared to the neighboring wild type (blue star), DE-Cad levels in *α-tat-*
332 *RNAi* cell boundaries are thicker (red stars).
333 (**C**, **D**) Likewise, thickening of the Cadherin (DE-Cadherin antibody) at cell boundaries was
334 also seen in *α-tat*-RNAi expressing somatic clones in MAG squamous epithelium from a 10-
335 day-old adult. In both control (C) and test (D), somatic clones (nuclear GFP) are marked by
336 red stars.
337 (**E, F**) A comparison of cofilin (white/grey, E) and actin (phalloidin, green/grey, F) between
338 control and somatic clones with *α-tat* knockdown (green nuclei, E and blue nuclei, F; also
339 marked by broken lines) in the follicular epithelium of stage 14 oocytes.
340 (**G**) Characteristics of Life-act GFP (grey) expression pattern in adult MAG epithelium and
341 upon *α-tat* knockdown.
342 (**H**) Schematic summarizing the cytoskeletal defects resulting from loss of microtubule
343 acetylation.
344 Scale bars: (A-F) 10 µm, (G) 50 µm
345
346 **Figure 3. Yki linked TOR signaling regulate microtubule acetylation in squamous**
347 **epithelia**.
348 (**A**, **B**) *α-tat* knockdown leads to persistent nuclear localization of Yki-GFP in both MAG
349 (*ov>α-tat-IR*, A) and follicle (RFP negative cells, *hs-flp, act>a-tat-IR*, B) epithelia.
350 (**C**, **D**) *yki* knockdown increases acetylated microtubule (acet-MT, grey) levels in the MAG
351 epithelium (D) compared to control (C).
352 (**E**) The elevation of acetylated microtubules caused by *yki* knockdown (*ov>yki-IR*, middle
353 panel) is reversed by simultaneous *α-tat* knockdown *(ov>α-tat-IR; yki-IR,* right panel).
354 (**F-H**) *yki* knockdown in the MAG epithelium increases cell area (F, G). Simultaneous
355 knockdown of *yki* and *α-tat* restores MAG cell area (right panel, see quantification in G),
356 besides adult survival (Kaplan-Meier plot, H). This phenotype and reduced adult survival (H)
357 are rescued by co-knockdown of *α-tat*.
358 (**I**, **J**) *yki* knockdown in the follicle epithelium (*GR1>yki-IR*) (J) reduces acetylated
359 microtubule levels compared to control (I).
360 (**K-N**) Gain of TOR signaling (via *myr-Akt*) elevates acetylated microtubules (acet-MT) in
361 both MAG (*ov>myr-Akt*, K) and follicle (*c204>myr-Akt*, L) epithelia, while loss of TOR
362 signaling (via *Akt-IR*) reduces it (*ov>Akt-IR*, M; *c204>Akt-IR*, N).
363 Data analyzed by unpaired *t*-test (****$p<0.0001$, ***$p=0.0008$). *n* values indicate cells; N=3
364 Scale bars: 10 µm (A, E, F); 50 µm (B-D, I-N).

365 **Figure 4: Distinct mechanical contexts drive differential Yki and TOR signaling in**
366 **squamous epithelia of MAG and choriogenic follicular cells**
367 (**A**) UMAP visualization of integrated single-cell transcriptomes from wild-type adult male
368 accessory gland (MAG) and ovary. Cells are color-coded by their previously annotated cell
369 types from the Fly Cell Atlas.
370 (**B**) UMAP of a subset containing only the squamous epithelial cells: choriogenic main body
371 follicle cells at Stage 14 (CMBFC-St.14) from the ovary and main cells from the MAG
372 (MAG-MC). This subset was used for comparative analysis of squamous epithelia from male
373 and female reproductive organs.
374 (**C**) Violin plots showing the expression levels of key genes from the TOR, Insulin, and
375 Hippo signaling pathways, identified through differential expression analysis between MAG-
376 MC and CMBFC-St.14 cells.
377 (**D**) Model of mechanical context-dependent Yki signaling outputs. The ovarian follicular
378 squamous epithelium (left) interfaces with a rigid apical chorion, while the MAG squamous
379 epithelium (right) faces a fluid-filled lumen. Knockdowns of the core mechanosensing
380 component, nuclear Yki signaling, lead to distinct phenotypes in these two mechanical
381 contexts: a squamous-to-cuboidal transition in the follicle epithelium, but squamous cell
382 carcinoma (SCC) in the MAG.

Figure 1

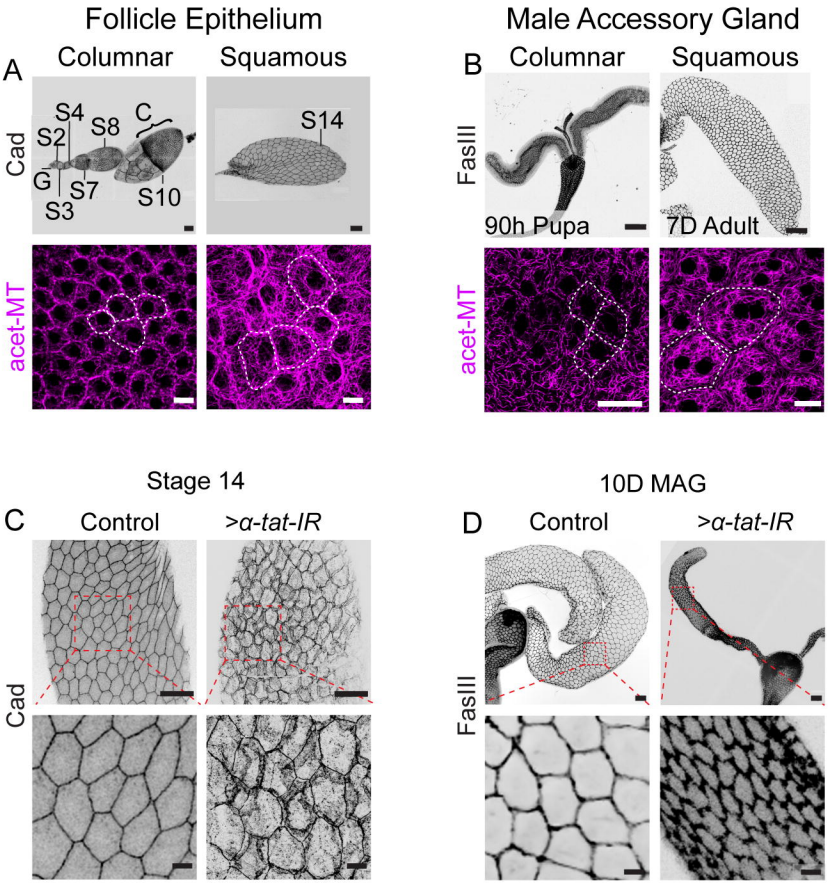
Follicle Epithelium
Male Accessory Gland
A
Columnar
Squamous
B
Columnar
Squamous
Cad
S4
S8
C
S2
G
S7
S3
S10
S14
FasIII
90h Pupa
7D Adult
acet-MT
acet-MT
Stage 14
10D MAG
C
Control
>α-tat-IR
D
Control
>α-tat-IR
Cad
FasIII

Figure 2

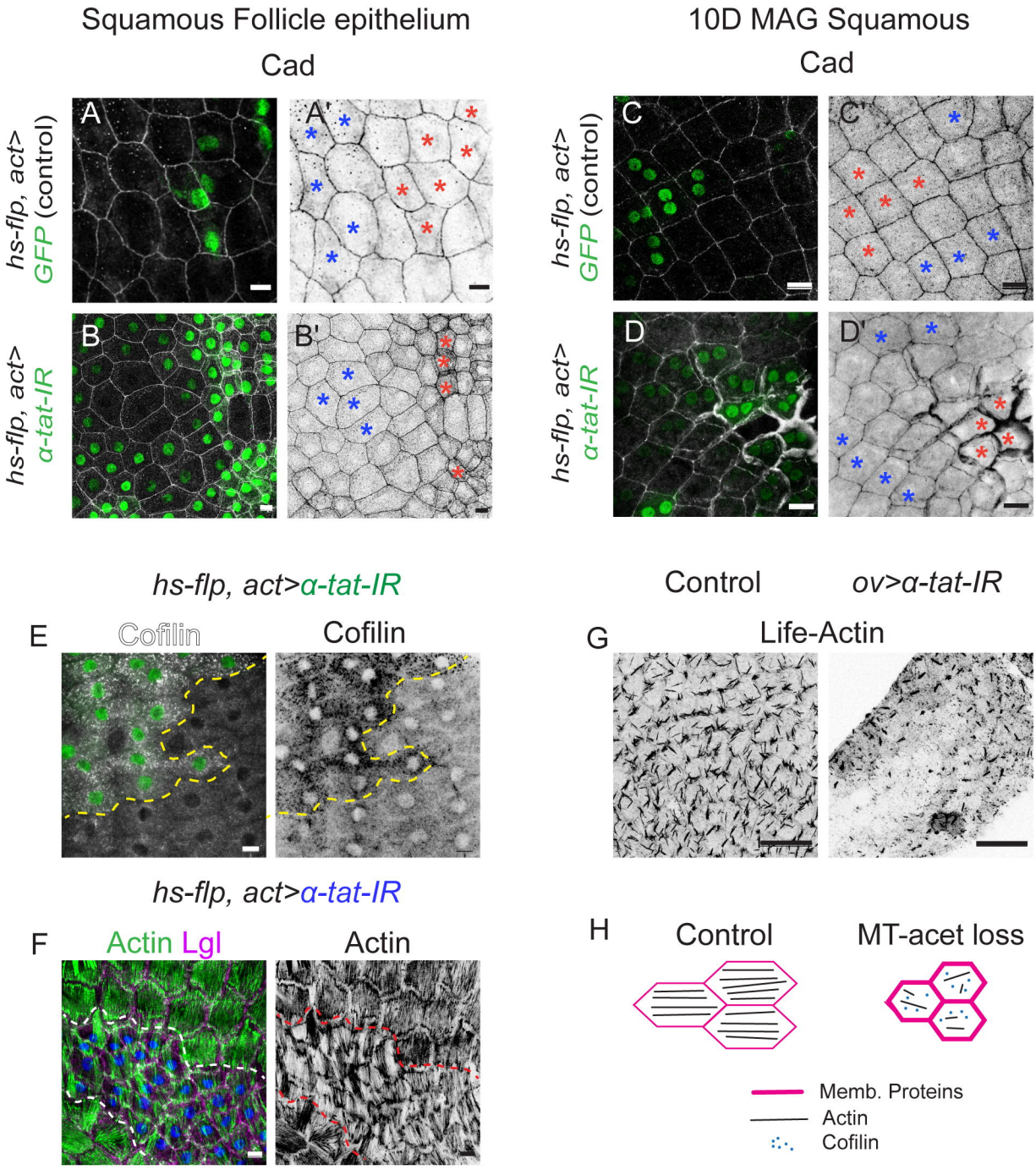
Squamous Follicle epithelium
Cad
10D MAG Squamous
Cad
hs-flp, act>
GFP (control)
hs-flp, act>
α-tat-IR
A
A'
B
B'
C
C'
D
D'
hs-flp, act>α-tat-IR
E
Cofilin
Cofilin
hs-flp, act>α-tat-IR
F
Actin Lgl
Actin
Control
ov>α-tat-IR
G
Life-Actin
H
Control
MT-acet loss
Memb. Proteins
Actin
Cofilin

Figure 3

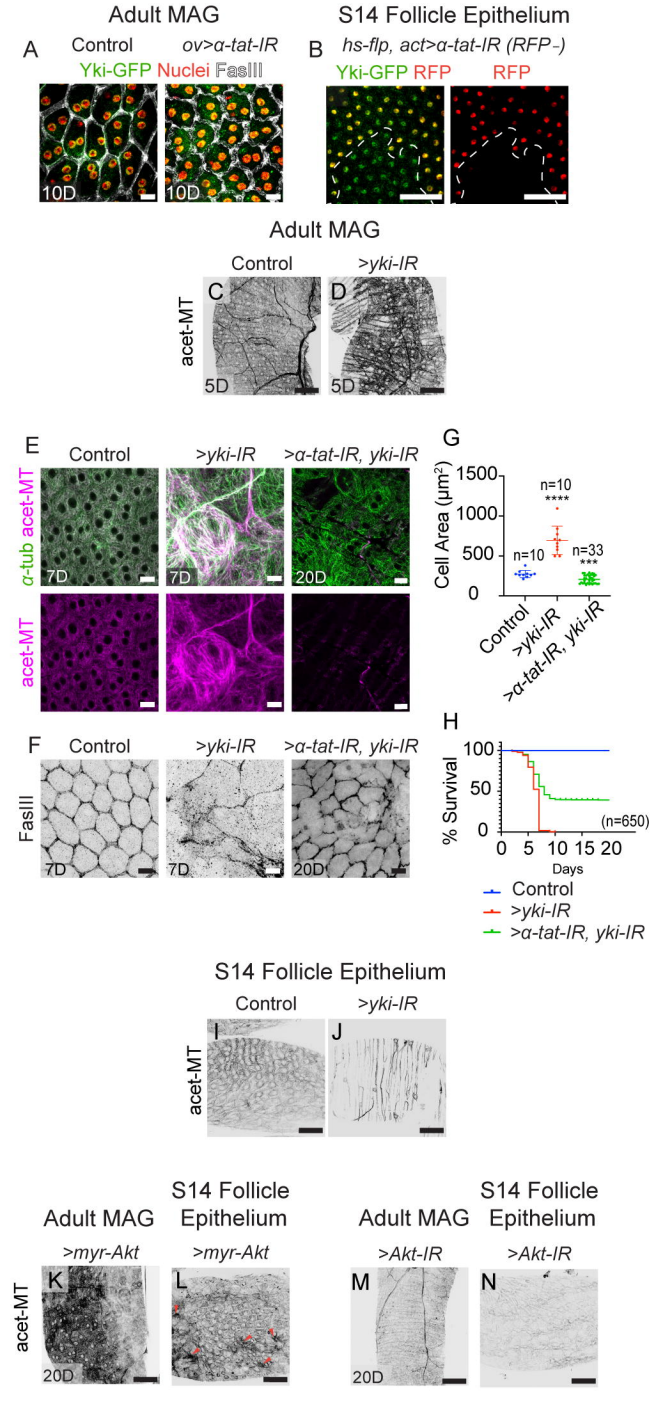
Adult MAG
S14 Follicle Epithelium
A
Control
ov>α-tat-IR
Yki-GFP Nuclei FasIII
10D
10D
B
hs-flp, act>α-tat-IR (RFP-)
Yki-GFP RFP
RFP
Adult MAG
Control
>yki-IR
acet-MT
C
D
5D
5D
E
Control
>yki-IR
>α-tat-IR, yki-IR
α-tub acet-MT
acet-MT
7D
7D
20D
G
Cell Area (μm²)
1500
1000
500
0
n=10
n=10
****
n=33
***
Control
>yki-IR
>α-tat-IR, yki-IR
F
Control
>yki-IR
>α-tat-IR, yki-IR
FasIII
7D
7D
20D
H
% Survival
100
50
0
(n=650)
0 5 10 15 20
Days
Control
>yki-IR
>α-tat-IR, yki-IR
S14 Follicle Epithelium
Control
>yki-IR
acet-MT
I
J
Adult MAG
S14 Follicle Epithelium
>myr-Akt
>myr-Akt
acet-MT
K
L
20D
Adult MAG
S14 Follicle Epithelium
>Akt-IR
>Akt-IR
M
N
20D

Figure 4

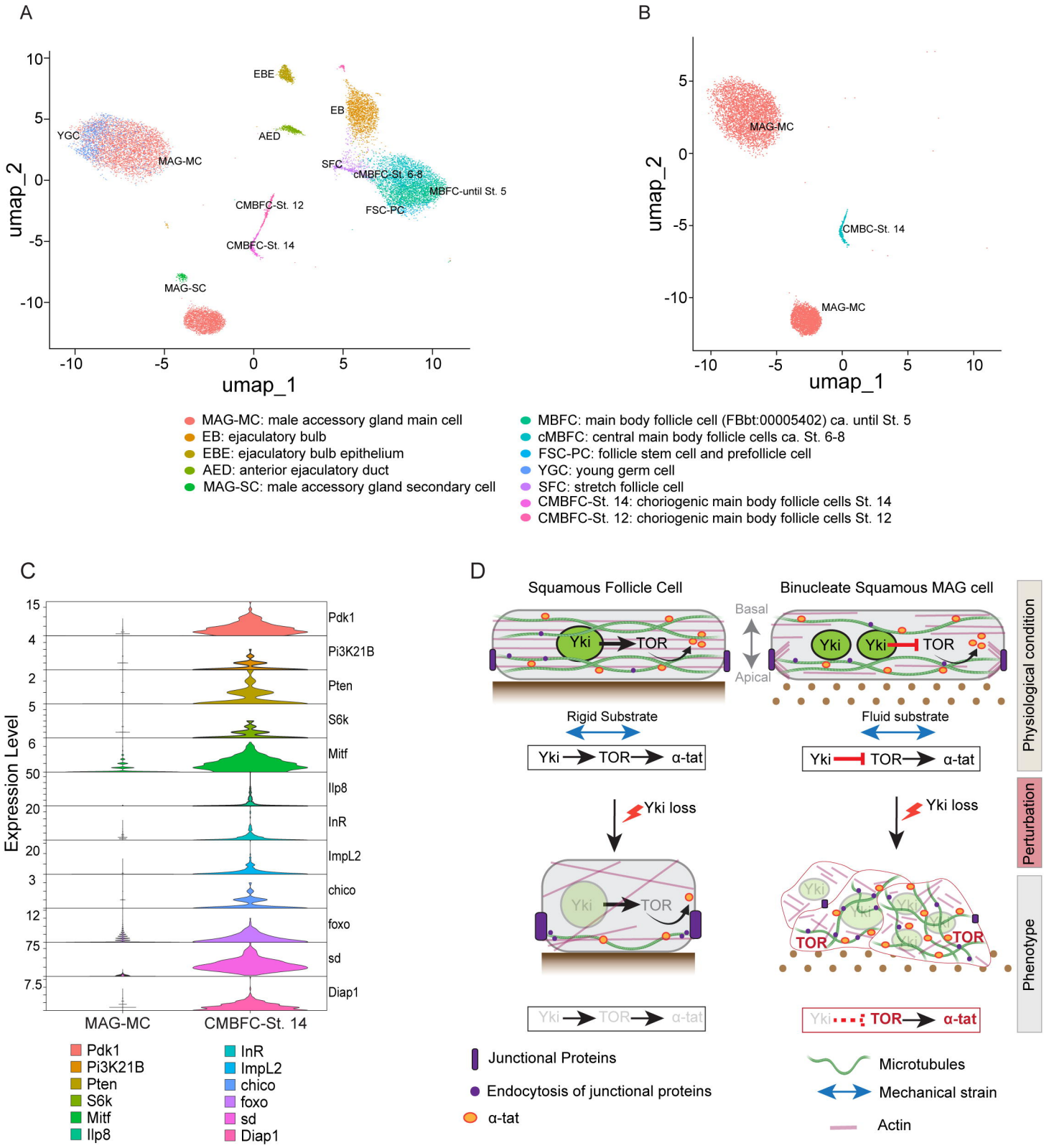
A
EBE
EB
YGC
AED
MAG-MC
SFC
cMBFC-St. 6-8
MBFC-until St. 5
CMBFC-St. 12
FSC-PC
CMBFC-St. 14
MAG-SC
umap_1
umap_2
B
MAG-MC
CMBC-St. 14
MAG-MC
umap_1
umap_2
MAG-MC: male accessory gland main cell
EB: ejaculatory bulb
EBE: ejaculatory bulb epithelium
AED: anterior ejaculatory duct
MAG-SC: male accessory gland secondary cell
MBFC: main body follicle cell (FBbt:00005402) ca. until St. 5
cMBFC: central main body follicle cells ca. St. 6-8
FSC-PC: follicle stem cell and prefollicle cell
YGC: young germ cell
SFC: stretch follicle cell
CMBFC-St. 14: choriogenic main body follicle cells St. 14
CMBFC-St. 12: choriogenic main body follicle cells St. 12
C
Expression Level
Pdk1
Pi3K21B
Pten
S6k
Mitf
Ilp8
InR
ImpL2
chico
foxo
sd
Diap1
MAG-MC
CMBFC-St. 14
Pdk1
Pi3K21B
Pten
S6k
Mitf
Ilp8
InR
ImpL2
chico
foxo
sd
Diap1
D
Squamous Follicle Cell
Binucleate Squamous MAG cell
Basal
Apical
Yki
TOR
Rigid Substrate
Fluid substrate
Yki → TOR → α-tat
Yki ⊣ TOR → α-tat
Yki loss
Yki loss
Yki → TOR → α-tat
Yki ⊣ TOR → α-tat
Physiological condition
Perturbation
Phenotype
Junctional Proteins
Endocytosis of junctional proteins
α-tat
Microtubules
Mechanical strain
Actin